Environmental Research 212 (2022) 113302

Contents lists available at ScienceDirect

Environmental Research

journal homepage: www.elsevier.com/locate/envres

Assessment of carbonaceous aerosols in suburban Nanjing under air pollution control measures: Insights from long-term measurements

Liang Dai [a], Lei Zhang [a], Dong Chen [c], Yu Zhao [a,b,*]

[a] State Key Laboratory of Pollution Control and Resource Reuse and School of the Environment, Nanjing University, 163 Xianlin Ave., Nanjing, Jiangsu, 210023, China
[b] Jiangsu Collaborative Innovation Center of Atmospheric Environment and Equipment Technology (CICAEET), Nanjing University of Information Science and Technology, Jiangsu, 210044, China
[c] Jiangsu Provincial Academy of Environmental Science, 176 North Jiangdong Rd., Nanjing, Jiangsu, 210036, China

ARTICLE INFO

Keywords:
Primary organic carbon
Secondary organic carbon
Air quality
Backward trajectory

ABSTRACT

The concentrations of organic carbon (OC) and elemental carbon (EC) in fine particulate matter ($PM_{2.5}$) were analyzed using a semicontinuous carbon analyzer to characterize their carbonaceous components at the Nanjing University site from August 2013 to December 2018. OC was divided by the minimum R squared (MRS) method into primary organic carbon (POC) and secondary organic carbon (SOC). The results showed that annual mean POC and EC concentrations declined from 10.00 to 3.62 μg m^{-3} and from 6.73 to 3.40 μg m^{-3}, respectively, during 2013–2018. The apparent reduction in POC and EC concentrations indicated that the implementation of air pollution control measures helped reduce carbonaceous aerosol pollution. Higher concentrations of POC and EC were recorded during the cold season and lower in the warm season. The annual mean SOC concentrations varied between 4.35 and 3.18 μg m^{-3} from 2013 to 2018. Elevated SOC was observed during the warm season, most likely attributable to the enhanced photochemical activity at high temperatures. Regarding the diurnal variation, the high concentrations of POC and EC were observed at night and in the morning due to stronger primary emissions and accumulations of pollutants with low boundary-layer heights, while the peak of SOC was observed at approximately noon due to the increases in photochemical activity. Nonparametric wind regression analysis showed the higher concentrations of POC, SOC and EC in the northwesterly, southwesterly to southeasterly, and southwesterly winds with high speeds. Concentration-weighted trajectory (CWT) analysis suggests that the areas with potentially high contributions to POC and EC changed from the north to the western areas of China, and that northern China played an increasingly important role in the SOC concentration of Nanjing. These results demonstrate that controlling emissions from the western and the northern areas in China may further alleviate carbonaceous aerosol pollution in Nanjing.

1. Introduction

Carbonaceous aerosols are major components of fine particulate matter ($PM_{2.5}$), (total carbon, TC) and can create challenges from local to global levels for air quality, including air quality, public health, and climate (Bond et al., 2013; Ding et al., 2013a; Vodicka et al., 2015). TC has two main subfractions, namely, organic carbon (OC) and elemental carbon (EC). Carbonate carbon (CC) may be negligible to the TC mass in fine $PM_{2.5}$ (Ji et al., 2016). EC is primarily generated from incomplete coal burning and vehicular exhaust. OC contains primary organic carbon (POC) and secondary organic carbon (SOC) and is highly diverse in its chemical composition. POC is considered to share similar sources to EC (Wang et al., 2015), while SOC is formed through the oxidation of volatile organic compounds (VOCs) (Chen et al., 2017; Yu, 2011; Zhang et al., 2017).

China has suffered severe aerosol pollution for the past decade, particularly in the economically developed eastern regions, such as the Yangtze River Delta, which has been attributed to high emissions of air pollutants from fast urbanization and industrialization, (YRD, Qi et al., 2015). As the capital of Jiangsu Province and one of the largest megacities in the YRD, Nanjing had a $PM_{2.5}$ concentration reaching 77.0 μg m^{-3} in 2013, 1.2 times the second-grade National Ambient Air Quality Standards (Wang et al., 2017). Facing the substantial challenge of air quality improvement, since 2013, China has conducted its toughest-ever

* Corresponding author. State Key Laboratory of Pollution Control and Resource Reuse and School of the Environment, Nanjing University, 163 Xianlin Ave., Nanjing, Jiangsu, 210023, China.
E-mail address: yuzhao@nju.edu.cn (Y. Zhao).

https://doi.org/10.1016/j.envres.2022.113302
Received 6 January 2022; Received in revised form 3 April 2022; Accepted 9 April 2022

air pollution control plan, aiming to reduce the $PM_{2.5}$ concentration by 20% within 5 years in the YRD (Jin et al., 2016; Zhang et al., 2019). As a result, the air quality in Nanjing improved significantly from 2013 to 2018 (http://hbj.nanjing.gov.cn/njshjbhj/201906/t20190605_1559172.html, last accessed: June 26, 2019). A series of studies on carbonaceous aerosols have been conducted in Nanjing, revealing interannual and seasonal variations of this important component of $PM_{2.5}$. From 2001 to 2014, the concentration of OC increased significantly from 5.6 to 13.4 μg m^{-3}, while that of EC stayed between 3.8 and 3.2 μg m^{-3} (An et al., 2015; Chen et al., 2017; Yang et al., 2005). From 2014 to 2017, the concentrations of OC and EC decreased significantly from 39.1 to 11.1 μg m^{-3} and from 5.7 to 0.9 μg m^{-3}, respectively (Liu et al., 2019; Wang et al., 2017), and the decreased TC concentration contributed to improved air quality in Nanjing (Wang et al., 2017). Carbonaceous aerosols pollution was more serious in the cold season (Ji et al., 2019a). The highest concentration of SOC occurred in winter, followed by autumn, summer and spring, while the ratio of SOC to OC was highest in summer (Li et al., 2015), indicating varied sources of carbonaceous aerosols in different seasons. Overall, previous studies have seldom focused on the impact of air pollution control measures.

To evaluate the effectiveness of air pollution control measures, it is very important to obtain the high-resolution concentrations of EC and OC for a long time sequence. Most previous studies relied on limited membrane sampling, which can reflect only the average concentration over a period of time (Bao et al., 2017; Hu et al., 2010; Huang et al., 2014; Li et al., 2015). Long-term measurements with a relatively high temporal resolution are essential for understanding the changing pattern under air pollution control measures. However, long-term measurements of OC and EC are still rare in China, and the effectiveness of emission controls on carbonaceous aerosol pollution alleviation remains unclear.

Nanjing is a typical city with a developed industrial economy and one of the pioneer cities that has implemented stringent emission control measures to reduce aerosol pollution over the past decade. The evolution of carbonaceous aerosol patterns in Nanjing, to a larger extent, exemplifies the progress of national action on air improvement. In this study, we reported the longest record of carbonaceous aerosols in Nanjing with semi-continuous measurements. The interannual, seasonal, weekly, and diurnal variations in POC, EC and SOC (estimated with the EC-tracer method) were investigated to elucidate their variation characteristics and assess the effectiveness of control measures taken in Nanjing. We further applied nonparametric wind regression (NWR), concentration-weighted trajectory (CWT) methods and backward trajectory clustering analysis to evaluate the impact of local and regional anthropogenic sources of carbonaceous aerosols. The study could help improve the understanding of the drivers of changing carbonaceous aerosols and the effectiveness of PM control measures on them.

2. Materials and methods

2.1. Description of the site

As shown inFigure S1, the measurements were conducted at a suburban site in the Xianlin Campus of Nanjing University (NJU). The instrument is located on the roof of School of Environment (118°57′10″E, 32°07′14″N, 30 m above ground), approximately 300 m away from the G25 highway and 20 km from downtown.Figure S2 in the supplement shows the wind rose plot for the NJU site during this period. Few emission sources of primary aerosols exist within 10 km of the site, and none are located upwind (Ding et al., 2013a). Air pollution in Nanjing is affected by multiple sources. Given the prevailing winds from the southeast and northeast, the site is located upwind of Nanjing and downwind of the Suzhou–Wuxi–Changzhou city cluster, one of the most developed regions in the YRD. Common air pollution control measures have been implemented simultaneously in the YRD region. Therefore, NJU can be considered a suburban site, which can reflect the mixed contributions of air pollutant emissions in Nanjing and the YRD region (Ding et al., 2013a). Due to the maintenance of the instrument in 2019 and the irregular effect of the novel coronavirus (2019-nCoV) epidemic lockdown, limited data were available from 2019 to 2020. Therefore, our dataset covers from August 1, 2013 to December 30, 2018.

2.2. Field measurements

Hourly ambient concentrations of OC and EC in $PM_{2.5}$ were sampled and analyzed by semicontinuous carbon analyzers (Model 4, Sunset Lab, USA). The analyzer used the National Institute of Occupational Safety and Healthy modified protocol (NIOSH 5040) as its default protocol to measure OC and EC. The airborne particles were injected into a $PM_{2.5}$ cyclone at a sampling flow rate of 8.0 L min^{-1}. $PM_{2.5}$ was collected using a circular 16 mm quartz filter. The sampling period was 40 min and the analysis process lasted for 15 min for each cycle (Chen et al., 2017). Before the $PM_{2.5}$ was collected by the quartz filter, the volatile organic gases were removed by a multichannel parallel plate denuder installed upstream of the analyzer. The sampled aerosols were repeatedly heated at four increasing temperature steps in different oxidizing atmospheres in the analysis chamber to evaporate carbon components with different forms. Then, the carbon components were catalytically oxidized to CO_2 gas in the oxidizing oven. All the carbon components (OC and EC) were converted to CO_2 and detected with a nondispersive infrared (NDIR) sensor. OC and EC were automatically quantified by standard methane gas (5% CH_4 in He). Although we operated the analyzer strictly according to standard operating procedures (SOPs, https://www3.epa.gov/ttnamti1/spesunset.html, last accessed: June 26, 2019), the data obtained by the analyzer were partially flawed due to uncontrollable factors. We removed defective data based on the following principles. 1) The random data points below the detection limit were treated as invalid data (0.5 μg m^{-3} for both OC and EC, https://www.sunlab.com/model-4-semi-continuous-oc-ec-field-analyzer/, last accessed: June 26, 2019). We removed the invalid values as suggested by Schmale et al. (2017). 2) When any data point was 10 times larger than its surrounding two points, we considered it an outlier and removed it. The percentage of data removed in each year was 16.7%, 12.9%, 11.0%, 15.3%, 17.3% and 18.6% for 2013, 2014, 2015, 2016, 2017 and 2018, respectively. In total, 28,234 h of OC and EC concentrations were available after screening. The concentrations of SO_2, O_3, CO, and NO_2 were measured by Thermo Environmental Instruments (Model 43i-TLE, 49i, 48i, and 42i). The $PM_{2.5}$ concentration was monitored using a Thermo Scientific TEOM 1405. The CSI-CR1000 automatic weather station was used to measure meteorological parameters, including wind speed, wind direction, relative humidity (RH), temperature (T) and solar radiation.

2.3. Wind analysis and source identification

2.3.1. Wind analysis

Developed by Henry et al. (2009), NWR combines ambient concentrations with measurements of wind direction and speed. The principle of NWR is to give weight to concentration values associated with wind direction (θ) and speed (u); the weighting coefficients are determined through Gaussian-like functions. The sustained wind incidence method (SWIM) consists of taking wind direction and speed standard deviations into account instead of constant smoothing parameters, as is done by the NWR (Vedantham et al., 2012). This allows us to dynamically "down-weight" data associated with high standard deviations. However, SWIM is only sensitive to high-value areas and not sensitive to low-to-medium values. Therefore, in this study, NWR was used to study the influence of wind speed and wind direction on pollutants. Analysis results were obtained using a new Igor-based tool, ZeFir, which enables a comprehensive investigation of the geographic origin of air pollutants (Petit et al., 2017). The method was discussed in detail by Petit et al. (2017). Briefly, the NWR graph represents an integrated picture of the relationships of

Table 1
Medians, averages, and associated standard deviations for the OC, EC, POC, SOC and $PM_{2.5}$ concentrations (in μg m^{-3}) from August 2013 to December 2018.

	OC			EC			POC			SOC			$PM_{2.5}$		
	Median	Average	SD	Median	Average	SD	Median	Average	SD	Median	Average	SD	Median	Average	SD
2013	7.16	9.54	7.56	5.99	6.73	3.20	8.33	10.00	5.44	2.55	4.35	5.19	70.00	93.96	74.19
2014	3.81	4.89	4.11	3.61	4.09	1.75	4.54	5.66	3.70	1.32	2.76	3.83	70.00	78.33	46.87
2015	6.91	7.84	4.44	3.19	3.71	2.02	3.82	4.64	2.88	2.91	3.57	2.92	43.00	53.15	42.40
2016	7.98	8.71	3.99	3.89	4.41	2.00	4.19	5.00	2.86	3.48	3.91	2.61	34.00	43.73	36.03
2017	8.13	9.15	4.25	3.7	4.27	2.65	2.25	2.97	2.67	5.67	6.21	4.19	40.00	44.81	29.10
2018	6.11	6.68	2.99	2.98	3.40	1.70	2.94	3.62	2.29	2.94	3.18	1.84	34.00	47.45	41.98
Whole period	6.47	7.48	4.79	3.64	4.24	2.31	3.80	4.70	3.37	3.17	3.93	3.28	47.00	59.31	48.44

estimated concentrations of the specific pollutant, wind direction and wind speed. The graph of the joint probability for the wind data, similar to the wind rose graph, shows the occurrence probability distribution of the wind speed and wind direction.

2.3.2. Source identification

Identifying the sources of air pollution is important to evaluate the effectiveness of air pollution control plans. Both potential source contribution function (PSCF) and CWT can be used to investigate the sources of air pollutants. Compared to PSCF, CWT can distinguish the calculated pollutant concentrations in a grid cell, which is slightly higher or extremely higher than the given criterion. Therefore, CWT analysis was applied, as is was capable of distinguishing moderate sources from strong sources. The impact of pollutant transport was analyzed using backward trajectory clustering. In this study, the domain for the CWT and backward trajectory clustering was set in the range of (20–65° N, 65–150° E) with a grid cell size of 0.25° × 0.25°. The potential location responsible for high concentrations observed at the receptor site was detected from geographically identified air parcels with high concentrations of air pollutants and long residence times. The 48-h air mass backward trajectories reaching the sampling site were calculated using the Hybrid Single Particle Lagrangian Integrated Trajectory (HYSPLIT) model. The driven data (1° × 1° latitude-longitude horizontal resolution) introduced into the HYSPLIT model (September 2019, Version 4.2.0) were downloaded from the Global Data Assimilation System (ftp://arlftp.arlhq.noaa.gov/pub/archives/gdas1/). The model was run every hour of the day with an initial height of 100 m above the ground level (Ding et al., 2013b).

2.4. Estimation of $(OC/EC)_{pri}$

SOC and POC can be separated from OC by applying EC as a tracer (Turpin and Huntzicker, 1995; Wu et al., 2019). Based on the hourly data from online measurement, we applied Eqs. (1) and (2) to estimate SOC and POC concentrations:

$$SOC = OC - EC \times (\frac{OC}{EC})_{pri} \quad (1)$$

$$POC = OC - SOC \quad (2)$$

where OC and EC are the measured ambient OC and EC concentrations, respectively, and $(OC/EC)_{pri}$ is the ratio of primary OC to EC emissions with the contribution of SOC excluded (Wu et al., 2018).

$(OC/EC)_{pri}$ is the key parameter in the SOC calculation with the EC-tracer method. Traditionally, $(OC/EC)_{pri}$ was determined by various methods including the OC to EC ratio from the emission inventory, the lowest OC to EC concentration ratio during the observation, and the OC to EC concentration ratio at night (Guo et al., 2012, 2014; Huang et al., 2012). Millet et al. (2005) proposed the minimum R squared (MRS) method, which proved more robust in SOC estimation than the minimum OC/EC or percentile OC/EC method. Sandrini et al. (2014) and Cesari et al. (2018b) concluded that differences in emission sources in different seasons would lead to changes in $(OC/EC)_{pri}$. Based on the MRS method, we used a computer program developed by Wu et al. (2018) to calculate SOC, which calculated the $(OC/EC)_{pri}$ values separately for each season of each year. $(OC/EC)_{pri}$ obtained by the MRS method was close to those determined by the lowest OC to EC concentration ratio during the observation in Nanjing for the same season of the same year (Figure S3) (Chen et al., 2017; Li et al., 2015).

3. Results and discussion

3.1. Data overview

Table 1 summarizes the statistics of the POC, SOC, OC and EC concentrations from August 1, 2013 to December 30, 2018. Throughout the research period, the average hourly OC and EC concentrations were observed at 7.48 ± 4.79 and 4.24 ± 2.31 μg m^{-3}, contributing 15.0% and 8.3% to the $PM_{2.5}$ mass, respectively. The average concentrations of POC and SOC were 4.70 ± 3.37 and 3.93 ± 3.28 μg m^{-3}, respectively. Table S1 summarizes the interannual variation in meteorological parameters and atmospheric self-purification capacity (ASPC, shown in Table S1 in the supplement) during the study period. ASPC, which is a synthetic parameter connecting dilution by ventilation with wet scavenging (Tang et al., 2019), can be calculated according to the national standard "Atmospheric Self-purification Capacity Level" (GB/T34299-2017) (Dong et al., 2018). The wind speed and ASPC increased from 1.54 m s^{-1} to 1.49 in 2013 to 1.70 m s^{-1} and 2.21 in 2018. Previous studies showed that higher wind speeds were beneficial for reducing $PM_{2.5}$ concentrations, but no clear quantitative relationship between them was demonstrated (Chang et al., 2017; Ji et al., 2019b). Unlike wind speed, Tang et al. (2019) found that the relationship between ASPC and $PM_{2.5}$ concentration was negative. This indicates that the improvement of ASPC is beneficial to reducing the $PM_{2.5}$ concentration. The correlation between ASPC and $PM_{2.5}$ concentrations is between −0.63 and −0.25 ($P < 0.01$) (Table S1), which is close to the literature values (Dong et al., 2018; Tang et al., 2019). The increasing wind speed and ASPC led to a decline in annual average carbonaceous aerosol concentrations.Table S2 summarizes the interannual variations in gross domestic product (GDP), population, vehicle numbers, fossil fuel and electricity consumption in Nanjing. Compared with 2013, the 2018 consumption of coal, gasoline and diesel oil in 2018 declined by 10.5, 47.3 and 29.3%, while that of natural gas and electricity increased by 15.1 and 22.6%, respectively. The decreased fossil fuel use and increased clean energy use reduced EC and OC emissions and thereby reduced EC and OC concentrations (Tong et al., 2020).

Based on to the national air quality standard, six pollution levels were determined according to daily $PM_{2.5}$ concentration, i.e., excellent ($0 < PM_{2.5} \leq 35$ μg m^{-3}), good ($35 < PM_{2.5} \leq 75$ μg m^{-3}), lightly polluted (LP, $75 < PM_{2.5} \leq 115$ μg m^{-3}), moderately polluted (MP, $115 < PM_{2.5} \leq 150$ μg m^{-3}), heavily polluted (HP, $150 < PM_{2.5} \leq 250$ μg m^{-3}), and severely polluted (SP, $PM_{2.5} > 250$ μg m^{-3}). There were 9792, 10,271, 1175, 4580, 1628, and 224 h for the excellent, good, LP, MP, HP, and SP polluted periods, respectively. In total, 37% and 27% of the observed $PM_{2.5}$ concentrations exceeded China's first grade (35 μg m^{-3}) and the second grade National Ambient Air Quality Standard (75 μg

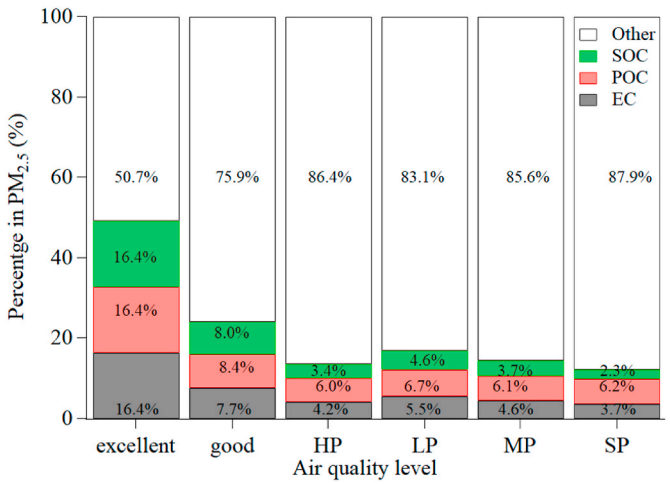

Fig. 1. Variation in average percentages of POC (red), SOC (green), EC (black) and other (white) components in $PM_{2.5}$ for different air quality levels. (For interpretation of the references to color in this figure legend, the reader is referred to the Web version of this article.)

m^{-3}), respectively. Fig. 1 shows the average percentages of POC, SOC, EC and other components in $PM_{2.5}$ under different pollution conditions. TC was the major component of $PM_{2.5}$ when the air quality was excellent and good, with its fraction reaching 49.3% and 24.1%, respectively. When the air quality became poor, other species dominated the $PM_{2.5}$ mass. In particular, TC contributed a small fraction (12.1%) of $PM_{2.5}$ during the SP period ($PM_{2.5} > 250\ \mu g\ m^{-3}$). This result indicates that the rapid accumulation of other compounds might be responsible for the poor air quality, which has been found in many cities in China (Guo et al., 2010).

3.2. Interannual variations

The relationship between OC and EC is an important indicator for understanding the source and chemical conversion of carbonaceous aerosols (Chen et al., 2017; He et al., 2010; Hu et al., 2012). Fig. 2 shows the relationships between OC and EC from 2013 to 2018. Except for 2017, OC and EC were well correlated, with R^2 ranging from 0.35 to 0.53. The good correlations indicate that OC and EC shared certain similar sources. Based on Table 1, the contribution of SOC to TC was highest in 2017 (46.3%) and lowest in 2013 (26.7%). We found that SOC accounted for a smaller fraction of TC when the correlation between OC and EC was stronger (Fig. 2). Meanwhile, the slopes between OC and EC decreased year by year (2013: 2.61, 2014: 2.57, 2015: 2.73, 2016: 2.3, 2017: 2.27, 2018: 2.12). This may be related to the small boiler shutdowns and large boiler upgrades.

Based on Table 1, the average annual mean concentrations of POC and EC decreased from 10.00 to 6.73 $\mu g\ m^{-3}$ in 2013 to 3.62 and 3.40 $\mu g\ m^{-3}$ in 2018, respectively. The largest decline in POC and EC concentrations was found during 2013–2014, with relative reductions of 45.3% and 36.9% between the two years, respectively (Table 1). From 2014 to 2018, the average annual decreasing rates of POC and EC concentrations were approximately 5.9% and 2.8%, respectively. As illustrated in Figure S4, many air pollution control measures were taken between 2013 and 2017. In 2013, Nanjing renovated 156 high-polluting enterprises, then renovated approximately 55 high-polluting enterprises every year over the following years (NJNBS, 2018). From 2013 to 2018, gasoline, diesel oil and coal consumption fell by 47.31, 29.28 and 10.51%, respectively (based onTable S2), which led to a reduction in EC and POC emissions. Table S3 summarizes the annual and seasonal variations in EC and OC emissions from 2013 to 2017 in Nanjing. The emissions of OC and EC showed a decreasing pattern, especially in the industrial sector. Based onTable S3, the ratio of OC to EC remained stable overall, but the ratio of OC to EC in the industrial sector showed a downward trend. Therefore, the treatment of high-polluting enterprises

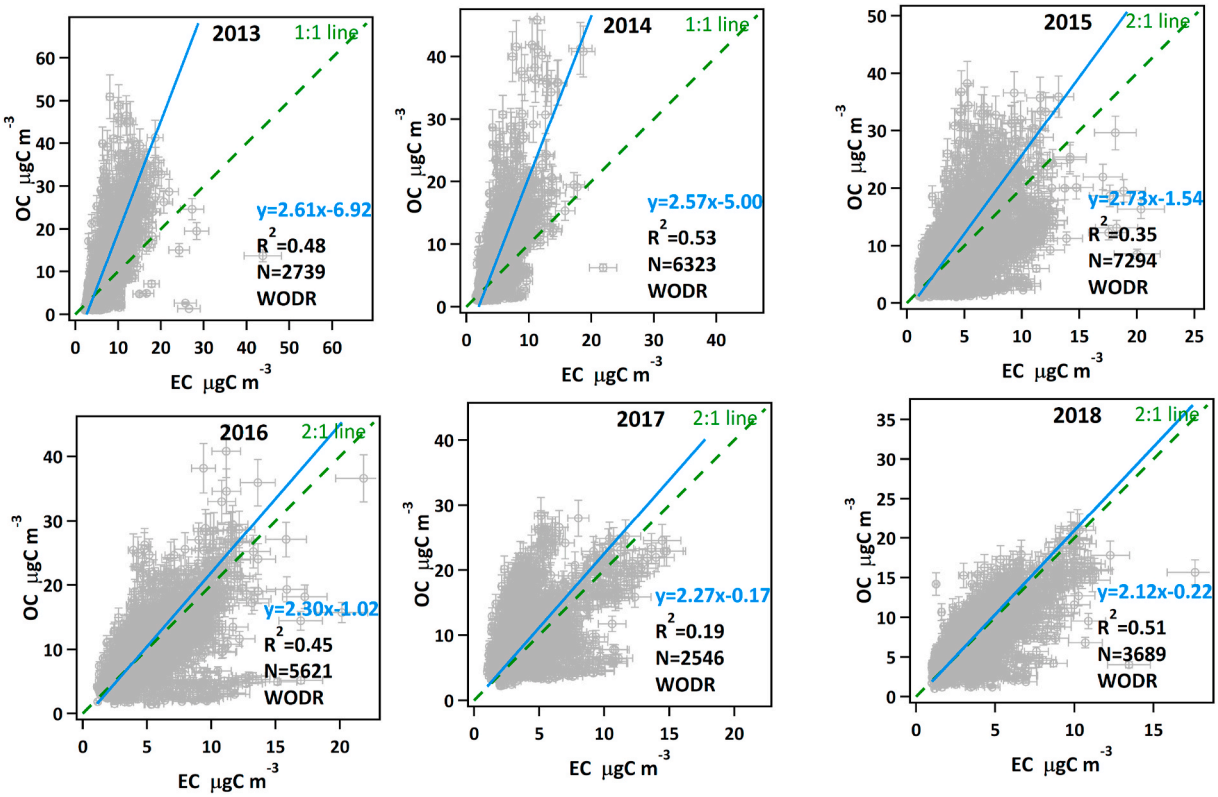

Fig. 2. Relationship between OC and EC using the Weighted orthogonal distance regression method from 2013 to 2018 (the dashed line indicates the OC/EC ratio).

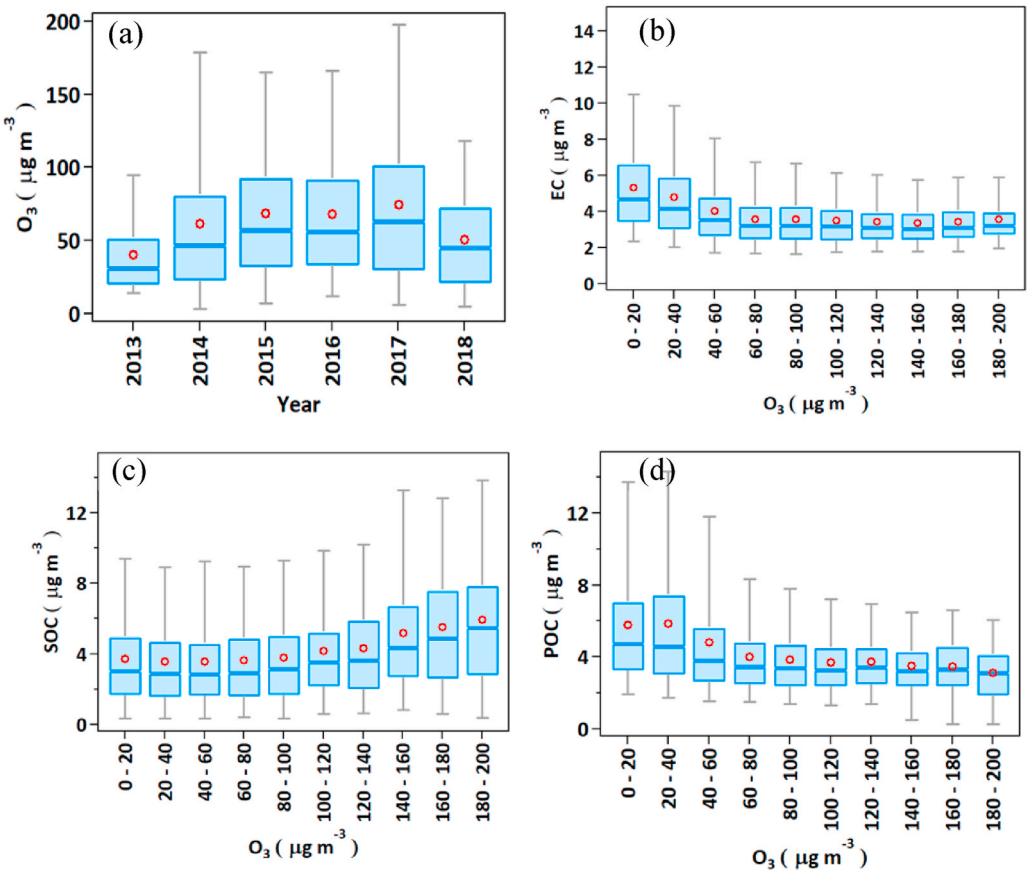

Fig. 3. Variation in the annual mean O_3 (a) and POC (b), SOC (c) and EC (d) concentrations as a function of the O_3 concentration during the study period. The mean (circle), median (horizontal line in the box), 25th and 75th percentiles (lower and upper ends of the box) and 10th and 90th percentiles (lower and upper whiskers) are shown.

could be responsible for the decreased POC and EC concentrations, suggesting the effectiveness of pollution control measures. In summary, the results from field measurements jointly gave credence to the assumption that POC and EC in Nanjing decreased in general from 2013 onwards due to upgraded energy consumption.

However, the SOC concentration did not decline significantly. As a secondary pollutant, SOC formation is influenced by many factors, such as solar radiation, precursor emissions, and atmospheric oxidation capacity. As illustrated in Figure S5, the daytime solar radiation value remained basically the same between 2013 and 2018. The VOCs emissions in Nanjing ranged from 136 to 141 kilo tons yr^{-1} with limited interannual change from 2013 to 2017 (http://meicmodel.org, last accessed: June 26, 2021). Therefore, the SOC level could be influenced by the changing atmospheric oxidation capacity. The annual averages of O_3 concentrations and the SOC, POC and EC concentrations by O_3 level are shown in Fig. 3. The O_3 concentration increased at a rate of 2.6 μg m^{-3} y^{-1} from 2013 to 2018, indicating enhanced atmospheric oxidative capacity (Fig. 3a). While EC and POC declined with O_3 growth (Fig. 3b and d), SOC concentration increased with it when the O_3 level was over 40 μg m^{-3}, at a rate of 1.1 μg m^{-3} per 50 μg m^{-3} growth of O_3. In summary, the limited reduction in VOCs emissions and the enhancement of atmospheric oxidation capacity could explain the slight increase in SOC concentrations since 2013.

3.3. Monthly and seasonal variations

The monthly and seasonal variations in POC, SOC and EC concentrations are illustrated in Fig. 4. The average POC and EC concentrations ranged from 2.0 (March 2017) to 16.9 μg m^{-3} (December 2013) and from 2.4 (August 2018) to 8.8 μg m^{-3} (December 2013), respectively. Similar variations were observed, with higher average concentrations of POC and EC in the cold season (from November to February of the following year) and lower concentrations in the warm season. The lowest and highest average concentrations for POC and EC commonly occurred in July and December during the whole period, respectively (Fig. 4a). The concentrations of POC and EC are affected by diffusion and rainwater removal, which has been observed in many cities (Chang et al., 2017). As shown inFigure S6, the average height of boundary layer (BLH) in July was 21.9% higher than that in December. Moreover, the highest average precipitation in July reached 16.9 mm, which was 3.7 times higher than that of December (Figure S7). The adverse diffusion (smaller BLH) and removal conditions (less precipitation) in December elevated the POC and EC concentrations (Ding et al., 2016). As a secondary pollutant, the monthly pattern of SOC concentration was different from that of POC and EC. The SOC concentration was higher in the warm season (from April to October) and lower in the cold season. The average SOC concentration ranged from 0.4 (August 2014) to 13.6 μg m^{-3} (May 2017). The lowest (2.3 μg m^{-3}) and highest monthly concentrations of SOC (6.7 μg m^{-3}) were observed in February and May throughout the period, respectively (Fig. 4a). Stronger solar radiation could be the reason for the high concentration in May (Figure S8), as it promotes the chemical conversion of VOCs to SOC (Zhao et al., 2015). In addition to the photochemical activity, another reason may be the higher emissions of SOC precursors (e.g., aromatics) in the summer (Wang et al., 2020). For example, Wang et al. (2020b) found that the emissions of aromatics in Nanjing in summer were about 10% higher than that in winter. Opposite patterns, i.e., elevated SOC in winter, were observed in some background sites, where biomass burning in winter played a more important role (Cesari et al., 2018a; Mousavi et al., 2019). Additionally, the SOC concentrations gradually decreased from May to

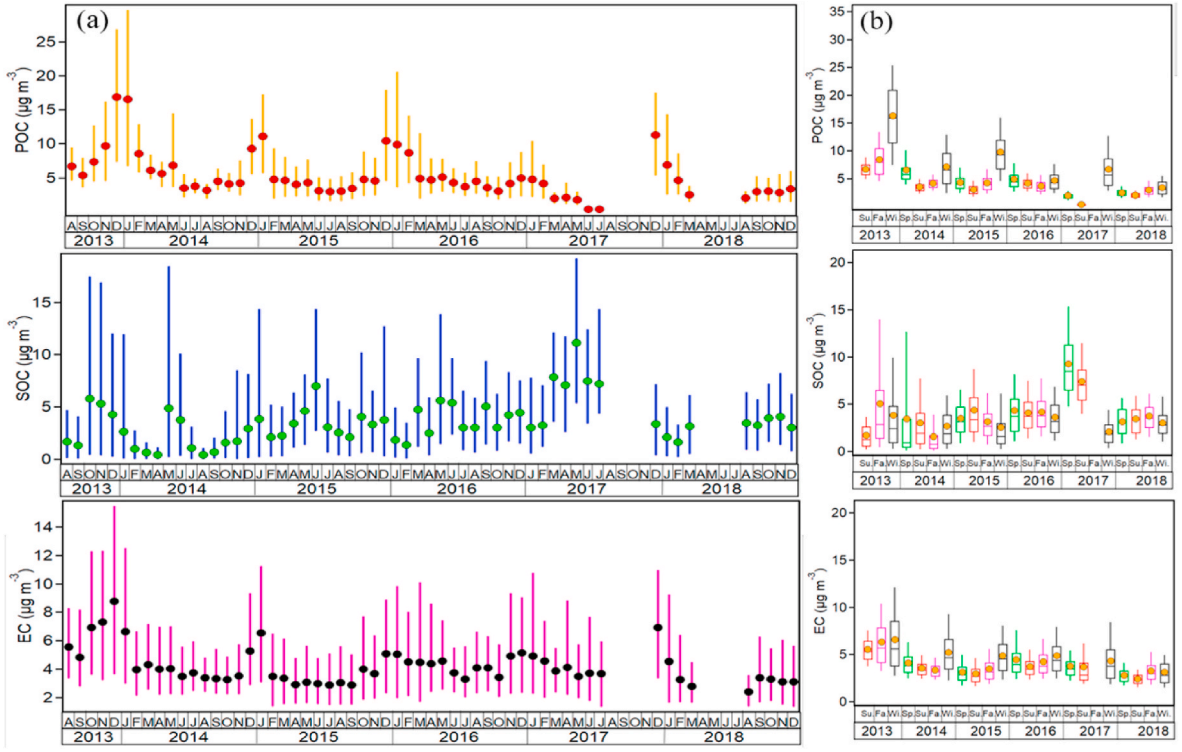

Fig. 4. Monthly (a) and seasonal (b) variations of POC, SOC and EC concentrations from August 2013 to December 2018. The mean (circle), median (horizontal line in the box), 25th and 75th percentiles (lower and upper ends of the box) and 10th and 90th percentiles (lower and upper whiskers) are shown.

August during the whole campaign (Fig. 4a). The increased temperature could lead to more semi-volatile organic compounds (SVOCs) remaining in the gas phase from May to August (Bao et al., 2017).

Higher EC emissions appeared in warmer seasons, which should increase the POC and EC concentrations during these periods (Table S3). However, the average concentrations of POC and EC in autumn and winter were usually higher, while those in spring and summer were lower. The highest average POC and EC concentrations were 16.3 ± 6.5 and 6.6 ± 3.6 μg m^{-3} in winter 2013, while the lowest was 0.4 ± 0.3 μg m^{-3} in summer 2017 and 2.4 ± 0.7 μg m^{-3} in summer 2018, respectively (Fig. 4b). The highest concentrations observed in winter could be caused by the adverse diffusion conditions and the stronger regional transport during winter (Ji et al., 2016). The large interquartile ranges of POC and EC in the cold seasons indicate significant accumulation processes in cold seasons. The SOC concentrations varied significantly by season. The large interquartile ranges of SOC for each season, especially summer and winter, indicate the cyclic accumulation and scavenging of air pollutants. Nanjing is located in a typical monsoon area, and the air masses arriving at the site by southeasterly/southwesterly winds in summer and by northerly/northwesterly winds in winter resulted in high levels of pollutants transported from the Pearl River Delta and North China Plain to the site (Ding et al., 2013b).

The differences in POC, SOC and EC concentrations in the warm and cold seasons decreased year by year. Higher differences in POC, SOC and EC in the cold season and warm season each year appeared in 2013, which were 12.78, 3.12 and 1.61 μg m^{-3}, respectively. The lowest differences in POC, SOC and EC in the cold season and warm season each year appeared in 2018, which were 1.22, 0.31 and 0.58 μg m^{-3}, respectively. This result implies that the pollution control measures implemented in recent years not only reduced the primary pollutants (POC and EC), but also started to limit the SOC precursors (VOCs).

3.4. Diurnal and weekend–weekday variations

Figures S9-S11 show the diurnal variations in POC, SOC and EC in different years. The diurnal patterns of POC and EC in this study exhibited two peaks: one during breakfast (6:00 to 9:00) and the other during dinnertime (18:00 to 20:00). Differently, In contrast, the diurnal variation in SOC concentration was unimodal (Figure S10). The maximum concentration of SOC appeared at approximately 12:00 (10:00–16:00) when solar radiation was the strongest (Lin et al., 2009). The first peak of POC and EC concentrations might be caused by the morning rush hour. The concentrations for POC and EC gradually decreased between 10:00 and 16:00, with the lowest at approximately 13:00. At this time, fewer cars were on the road, and emissions were weaker. Meanwhile, BLH was the highest at noon, which was most conducive to the diffusion of pollutants. The second peak of POC and EC concentrations might be caused by cyclic accumulation due to the decreasing BLH at night. The ratio of the highest to the lowest concentration within diurnal variation can be used to reflect the change in the source of the pollutant (Ji et al., 2019b). The peak concentrations during 17:00–09:00 of POC and EC were 1.82 and 1.53, 1.70 and 1.47, 1.37 and 1.40, 1.34 and 1.41, 1.38 and 1.52, and 1.31 and 1.41 times higher than the minimum concentrations observed during 10:00–16:00 for 2013, 2014, 2015, 2016, 2017 and 2018, respectively (Figures S9 and S11). We find that the ratio for POC dropped more significantly than that of EC. This result suggests that the reduction in POC emissions is more significant than that of EC. This was consistent with the fact that the POC concentration decreased faster than EC during the interannual variation (Table 1). The decreasing ratio reflected the increased combustion efficiency (Ji et al., 2019b). This might benefit from air pollutant control actions, such as shutting down small boilers and upgrading the combustion equipment of large boilers. The significant decline in the ratio for POC reflected that improving combustion efficiency more easily reduced emissions for POC than for EC. This is because EC is more heat-resistant than POC (Yu et al., 2010). For SOC, the maximum peak concentration was 2.35, 2.42, 1.18, 1.16, 1.21 and 1.15 times higher than the minimum concentration observed in the period 17:00–9:00 for 2013, 2014, 2015, 2016, 2017 and 2018, respectively. The ratio suddenly decreased in 2015 and remained relatively low afterward,

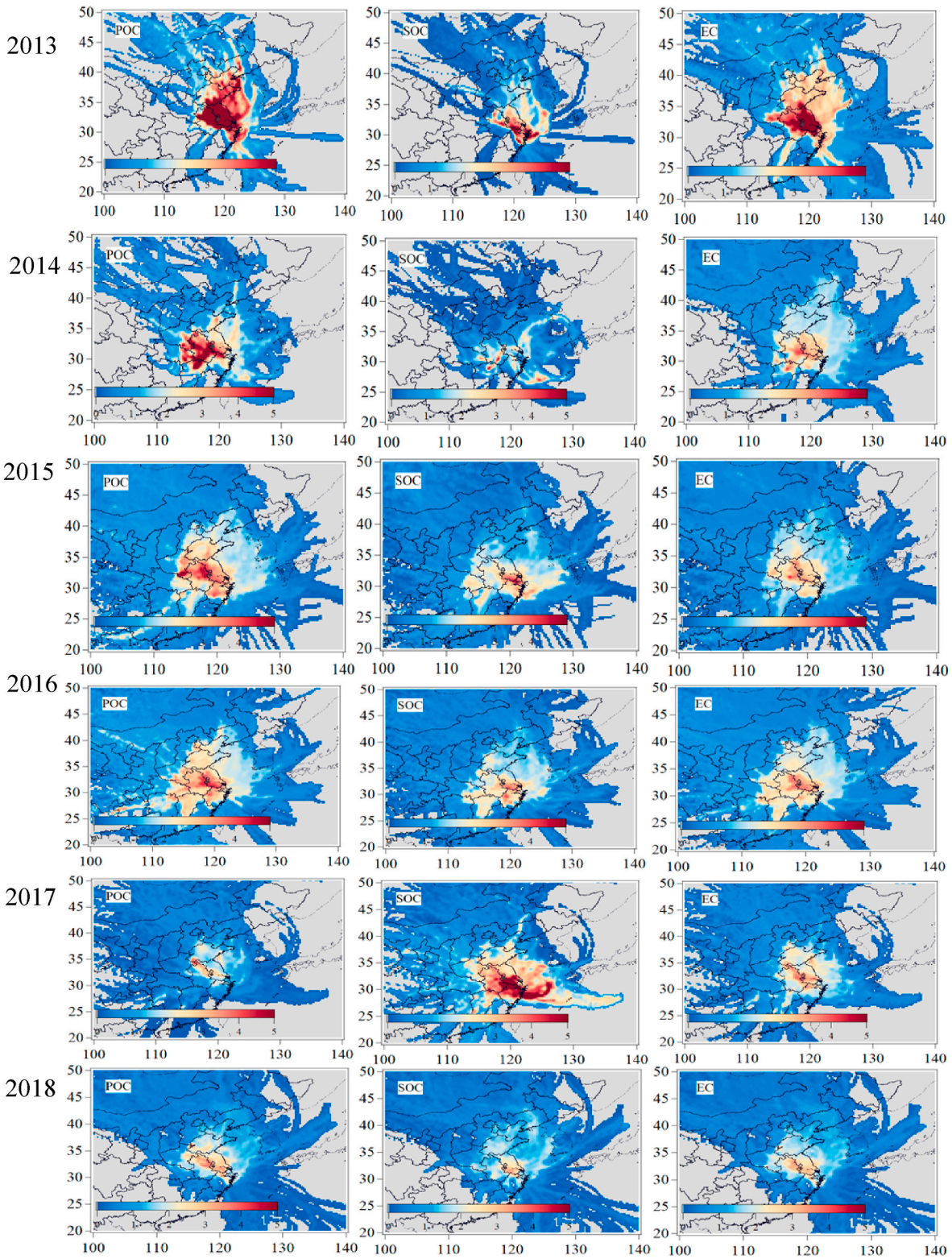

Fig. 5. Potential source areas for POC, SOC and EC in Nanjing from 2013 to 2018. The colorbar indicates the estimated concentration (μg m^{-3}).

indicating that the source of SOC in Nanjing changed significantly in 2015. This could be associated with the strengthened prohibition of straw burning and improved straw recycling (a recycling rate of 90% was reached by the local government) since 2015.

Previous studies have shown that the variations in carbonaceous aerosols during weekdays and weekends reflect the influence of anthropogenic activities (Ding et al., 2017; Huang et al., 2012, 2013; Wang et al., 2012). Figures S12-S14 show the diurnal patterns of POC, SOC and EC during weekdays and weekends. Except for SOC, the average concentrations of EC and POC declined for weekends and weekdays from 2013 to 2018. The average concentrations of EC for weekdays and weekends for 2013 were 6.6 μg m^{-3} and 7.1 μg m^{-3}, 0.93 and 1.08 times higher than those for 2018, respectively (Figure S14). The average concentrations of POC for weekdays and weekends for 2013

were 9.8 μg m^{-3} and 10.6 μg m^{-3}, respectively, which were 1.65 and 2.07 times higher than those for 2018, respectively (Figure S11). This indicates that POC and EC emissions control are efficacious, whether it is on weekdays or weekends. Similar diurnal variations in POC, SOC and EC were found on weekdays and weekends. The average POC, SOC and EC concentrations on weekdays were lower than those on weekends (Figures S12-S14). Correspondingly, the $PM_{2.5}$ concentrations on weekdays were lower than that those on weekends (Table S4). The increased outdoor excursions and corresponding transportation activities around the suburban site on weekends might have resulted in the stronger emissions and thereby elevated the ambient aerosol level. We performed two-tailed paired t-tests and proved that there was a difference between the concentrations of POC (t: 2.318 and sigm: 0.024) and SOC (t: 1.882 and sigm: 0.013) on weekdays and weekends ($p < 0.05$). It is possible that more outdoor activities on weekends elevated the emissions of POC and SOC precursors. The higher average concentrations of POC and EC for the weekend might be attributed to enhanced combustion processes, indicated by higher CO concentrations on the weekend (on average 0.97 ± 0.48 mg m^{-3} on weekdays and 1.01 ± 0.52 mg m^{-3} on weekend). There was no difference in EC (t: 1.882 and sigm: 0.065) concentration on weekdays and weekends, indicating no significant decline in emissions on the weekends compared to weekdays. This result is consistent with previous studies (Chang et al., 2017; Ji et al., 2018; Lin et al., 2009).

3.5. Impact of atmospheric transport

Figures S15-17 show the results of NWR analysis of POC, SOC, and EC concentrations in Nanjing from 2013 to 2018. NWR illustrated the hot spots (higher concentrations) of EC and POC in the northwest and southwest wind sectors at a wind speed of 6–15 km h^{-1}. The high concentrations of POC and EC were closely associated with regional transport (high wind speed) (Ji et al., 2019a). The POC and EC might be transported from the northwestern and southwestern areas of Nanjing. The hot spots of SOC appeared in the southeasterly to southwesterly sector at a wind speed of 5–15 km h^{-1} (Figure S16), indicating that SOC could be transported from the southwestern urban area of Nanjing and the YRD city cluster.

The cluster analysis of the backward trajectory indicates the concentration of pollutants carried by the polluted air mass and the areas where the polluted air mass passes. Figure S18 illustrates the air mass types and the POC, SOC and EC concentrations of each air mass from 2013 to 2018. The average POC and EC concentrations of air masses from northern China dropped from 8.1 to 5.2 μg m^{-3} in 2013 to 3.9 and 3.6 μg m^{-3} in 2018, respectively. The average POC and EC concentrations of air masses in Jiangsu Province dropped from 12.9 to 4.9 μg m^{-3} in 2013 to 4.1 and 3.8 μg m^{-3} in 2018. The average POC and EC concentrations of air masses from the coastal areas of southern China also decreased by approximately 41.3% and 53.5%, respectively. The results indicate that the air pollution control measures significantly reduced POC and EC concentrations in both southern and northern China (Ji et al., 2019b; Lu et al., 2021). In 2013, air masses with high SOC concentrations mainly came from northern Jiangsu Province. By 2018, high-concentration SOC air masses mainly came from northern China (Tianjin, Beijing, and Shandong). The average SOC concentration in the contaminated air masses in Jiangsu and the southeastern coastal area decreased from 5.9 to 5.2 μg m^{-3} in 2013 to 2.8 and 2.0 μg m^{-3} in 2018, respectively. In contrast, the reduction in air masses from northern China was limited from 3.5 in 2013 to 3.1 μg m^{-3} in 2018. The results suggest that the origin of SOC pollution in Nanjing in recent years might have switched to local areas and northern China.

Fig. 5 presents the CWT results for POC, SOC and EC during the study period. In 2013, the high-contribution areas of both POC and EC appeared mainly in northern China, and the high-contribution areas expanded to Hubei, Jiangxi and Hunan Provinces from 2013 to 2018. This indicates that the pollutant emissions from cities around Nanjing played a more important role in the air pollution of Nanjing along with the improved air quality across the country. The rapid economic growth, urbanization, increased industrial activity, and increased energy consumption in the northwestern and southwestern areas of Nanjing have resulted in high aerosol loads in downwind areas (Dai et al., 2018). In 2013, the area with a significant contribution to the Nanjing SOC concentration appeared in the surrounding areas of Nanjing. Over the following years, northern China had a large contribution of SOC concentration to Nanjing. Higher levels of aerosol and anthropogenic VOCs were reported in those areas (Li et al., 2019; Zheng et al., 2018).

In summary, the geographic origin of POC, SOC and EC in Nanjing has been changing. Economic development in western China has resulted in higher emissions in northwestern China, which in turn has elevated the carbonaceous aerosol level in Nanjing.

4. Conclusions

The hourly mass concentrations of OC and EC in $PM_{2.5}$ were measured semi-continuously at Nanjing University from August 1, 2013 to December 30, 2018, and POC and SOC were separated with the MRS method. POC and EC declined with the implementation of the air pollution control plan, while SOC concentration did not decrease significantly. To further improve air quality, precursors of SOC and secondary inorganic aerosols need to be controlled. The decreasing OC/EC indicates the improvement of energy use efficiency. The concentrations of POC and EC were higher in the colder months and lower in the warmer months, while the pattern of SOC was the opposite. The differences in POC, SOC and EC concentrations in the warm and cold seasons decreased year by year. The diurnal patterns of POC and EC were closely related to changes in emission sources and the evolution of the BLH. The higher POC and SOC levels could be attributed to enhanced anthropogenic emissions during the weekend.

Local emissions and regional transportation played an important role in TC concentrations. Higher values of POC, SOC, and EC appeared in the northwesterly, southeasterly, and mainly southwesterly and southeasterly wind sectors, respectively. This was consistent with their higher potential of source areas, as determined by the CWT analysis. The high contribution areas of POC and EC expanded from the north to the northwest and western regions of China, where coal and thermal power plants were abundant. The area with a high SOC contribution expanded from northern China. The reduced straw burning was beneficial to the decline in SOC concentration in Nanjing.

Declaration of competing interest

The authors declare that they have no known competing financial interests or personal relationships that could have appeared to influence the work reported in this paper.

Acknowledgments

This work was sponsored by the National Natural Science Foundation of China (41922052 and 42177080).

Appendix A. Supplementary data

Supplementary data to this article can be found online at https://doi.org/10.1016/j.envres.2022.113302.

References

An, J., Duan, Q., Wang, H., Miao, Q., Shao, P., Wang, J., Zou, J., 2015. Fine particulate pollution in the Nanjing northern suburb during summer: composition and sources. Environ. Monit. Assess. 187 (9), 561.

Bao, M.Y., Cao, F., Chang, Y.H., Zhang, Y.L., Gao, Y.Q., Liu, X.Y., Zhang, Y.Y., Zhang, W. Q., Tang, T.R., Xu, Z.F., Liu, S.D., Lee, X.H., Li, J., Zhang, G., 2017. Characteristics and origins of air pollutants and carbonaceous aerosols during wintertime haze

episodes at a rural site in the Yangtze River Delta, China. Atmos. Pollut. Res. 8, 900–911.
Bond, T.C., Doherty, S.J., Fahey, D.W., Forster, P.M., Berntsen, T., DeAngelo, B.J., Flanner, M.G., Ghan, S., Karcher, B., Koch, D., Kinne, S., Kondo, Y., Quinn, P.K., Sarofim, M.C., Schultz, M.G., Schulz, M., Venkataraman, C., Zhang, H., Zhang, S., Bellouin, N., Guttikunda, S.K., Hopke, P.K., Jacobson, M.Z., Kaiser, J.W., Klimont, Z., Lohmann, U., Schwarz, J.P., Shindell, D., Storelvmo, T., Warren, S.G., Zender, C.S., 2013. Bounding the role of black carbon in the climate system: a scientific assessment. J. Geophys. Res. Atmos. 118, 5380–5552.
Cesari, D., De Benedetto, G.E., Bonasoni, P., Busetto, M., Dinoi, A., Merico, E., Chirizzi, D., Cristofanelli, P., Donateo, A., Grasso, F.M., Marinoni, A., Pennetta, A., Contini, D., 2018a. Seasonal variability of $PM_{2.5}$ and PM_{10} composition and sources in an urban background site in Southern Italy. Sci. Total Environ. 612, 202–213.
Cesari, D., Merico, E., Dinoi, A., Marinoni, A., Bonasoni, P., Contini, D., 2018b. Seasonal variability of carbonaceous aerosols in an urban background area in southern Italy. Atmos. Res. 200, 97–108.
Chang, Y.H., Deng, C.R., Cao, F., Cao, C., Zou, Z., Liu, S.D., Lee, X.H., Li, J., Zhang, G., Zhang, Y.L., 2017. Assessment of carbonaceous aerosols in Shanghai, China - Part 1: Long-term evolution, seasonal variations, and meteorological effects. Atmos. Chem. Phys. 17, 9945–9964.
Chen, D., Cui, H.F., Zhao, Y., Yin, L.N., Lu, Y., Wang, Q.G., 2017. A two-year study of carbonaceous aerosols in ambient $PM_{2.5}$ at a regional background site for western Yangtze River Delta, China. Atmos. Res. 183, 351–361.
Dai, Q., Bi, X., Liu, B., Li, L., Ding, J., Song, W., Bi, S., Schulze, B.C., Song, C., Wu, J., Zhang, Y., Feng, Y., Hopke, P.K., 2018. Chemical nature of $PM_{2.5}$ and PM_{10} in Xi'an, China: insights into primary emissions and secondary particle formation. Environ. Pollut. 240, 155–166.
Ding, A.J., Fu, C.B., Yang, X.Q., Sun, J.N., Petaja, T., Kerminen, V.M., Wang, T., Xie, Y., Herrmann, E., Zheng, L.F., Nie, W., Liu, Q., Wei, X.L., Kulmala, M., 2013a. Intense atmospheric pollution modifies weather: a case of mixed biomass burning with fossil fuel combustion pollution in eastern China. Atmos. Chem. Phys. 13, 10545–10554.
Ding, A.J., Fu, C.B., Yang, X.Q., Sun, J.N., Zheng, L.F., Xie, Y.N., Herrmann, E., Nie, W., Petaja, T., Kerminen, V.M., Kulmala, M., 2013b. Ozone and fine particle in the western Yangtze River Delta: an overview of 1 yr data at the SORPES station. Atmos. Chem. Phys. 13, 5813–5830.
Ding, A.J., Huang, X., Nie, W., Sun, J.N., Kerminen, V.M., Petaja, T., Su, H., Cheng, Y.F., Yang, X.Q., Wang, M.H., Chi, X.G., Wang, J.P., Virkkula, A., Guo, W.D., Yuan, J., Wang, S.Y., Zhang, R.J., Wu, Y.F., Song, Y., Zhu, T., Zilitinkevich, S., Kulmala, M., Fu, C.B., 2016. Enhanced haze pollution by black carbon in megacities in China. Geophys. Res. Lett. 43, 2873–2879.
Ding, X.X., Kong, L.D., Du, C.T., Zhanzakova, A., Fu, H.B., Tang, X.F., Wang, L., Yang, X., Chen, J.M., Cheng, T.T., 2017. Characteristics of size-resolved atmospheric inorganic and carbonaceous aerosols in urban Shanghai. Atmos. Environ. 167, 625–641.
Dong, X., Liu, H., Tang, Z., Cao, J., Qiu, C., Center, S.C., 2018. Spatial-temporal characteristics of the atmospheric self-purification capacity index in the context of climate change in Shandong from 1961 to 2017. J. Mar. Meteorol. 38 (4), 93–102.
Guo, S., Hu, M., Guo, Q., Zhang, X., Zheng, M., Zheng, J., Chang, C.C., Schauer, J.J., Zhang, R., 2012. Primary sources and secondary formation of organic aerosols in Beijing, China. Environ. Sci. Technol. 46, 9846–9853.
Guo, S., Hu, M., Guo, Q.F., Shang, D.J., 2014. Comparison of secondary organic aerosol estimation methods. Hua Hsueh Hsueh Pao 72, 658–666.
Guo, S., Hu, M., Wang, Z.B., Slanina, J., Zhao, Y.L., 2010. Size-resolved aerosol water-soluble ionic compositions in the summer of Beijing: implication of regional secondary formation. Atmos. Chem. Phys. 10, 947–959.
He, L.Y., Lin, Y., Huang, X.F., Guo, S., Xue, L., Su, Q., Hu, M., Luan, S.J., Zhang, Y.H., 2010. Characterization of high-resolution aerosol mass spectra of primary organic aerosol emissions from Chinese cooking and biomass burning. Atmos. Chem. Phys. 10, 11535–11543.
Henry, R., Norris, G.A., Vedantham, R., Turner, J.R., 2009. Source region identification using kernel smoothing. Environ. Sci. Technol. 43, 4090–4097.
Hu, D., Bian, Q., Lau, A.K.H., Yu, J.Z., 2010. Source apportioning of primary and secondary organic carbon in summer $PM_{2.5}$ in Hong Kong using positive matrix factorization of secondary and primary organic tracer data. J. Geophys. Res. 115, D16204.
Hu, W.W., Hu, M., Deng, Z.Q., Xiao, R., Kondo, Y., Takegawa, N., Zhao, Y.J., Guo, S., Zhang, Y.H., 2012. The characteristics and origins of carbonaceous aerosol at a rural site of PRD in summer of 2006. Atmos. Chem. Phys. 12, 1811–1822.
Huang, H., Ho, K.F., Lee, S.C., Tsang, P.K., Ho, S.S.H., Zou, C.W., Zou, S.C., Cao, J.J., Xu, H.M., 2012. Characteristics of carbonaceous aerosol in $PM_{2.5}$: pearl delta river region, China. Atmos. Res. 104, 227–236.
Huang, R.J., Zhang, Y., Bozzetti, C., Ho, K.F., Cao, J.J., Han, Y., Daellenbach, K.R., Slowik, J.G., Platt, S.M., Canonaco, F., Zotter, P., Wolf, R., Pieber, S.M., Bruns, E.A., Crippa, M., Ciarelli, G., Piazzalunga, A., Schwikowski, M., Abbaszade, G., Schnelle-Kreis, J., Zimmermann, R., An, Z., Szidat, S., Baltensperger, U., El Haddad, I., Prevot, A.S., 2014. High secondary aerosol contribution to particulate pollution during haze events in China. Nature 514, 218–222.
Huang, X.F., Xue, L., Tian, X.D., Shao, W.W., Sun, T.L., Gong, Z.H., Ju, W.W., Jiang, B., Hu, M., He, L.Y., 2013. Highly time-resolved carbonaceous aerosol characterization in Yangtze River Delta of China: composition, mixing state and secondary formation. Atmos. Environ. 64, 200–207.
Ji, D., Gao, M., Maenhaut, W., He, J., Wu, C., Cheng, L., Gao, W., Sun, Y., Sun, J., Xin, J., Wang, L., Wang, Y., 2019a. The carbonaceous aerosol levels still remain a challenge in the Beijing-Tianjin-Hebei region of China: insights from continuous high temporal resolution measurements in multiple cities. Environ. Int. 126, 171–183.
Ji, D., Yan, Y., Wang, Z., He, J., Liu, B., Sun, Y., Gao, M., Li, Y., Cao, W., Cui, Y., Hu, B., Xin, J., Wang, L., Liu, Z., Tang, G., Wang, Y., 2018. Two-year continuous measurements of carbonaceous aerosols in urban Beijing, China: temporal variations, characteristics and source analyses. Chemosphere 200, 191–200.
Ji, D.S., Gao, W.K., Maenhaut, W., He, J., Wang, Z., Li, J.W., Du, W.P., Wang, L.L., Sun, Y., Xin, J.Y., Hu, B., Wang, Y.S., 2019b. Impact of air pollution control measures and regional transport on carbonaceous aerosols in fine particulate matter in urban Beijing, China: insights gained from long-term measurement. Atmos. Chem. Phys. 19, 8569–8590.
Ji, D.S., Zhang, J.K., He, J., Wang, X.J., Pang, B., Liu, Z.R., Wang, L.L., Wang, Y.S., 2016. Characteristics of atmospheric organic and elemental carbon aerosols in urban Beijing, China. Atmos. Environ. 125, 293–306.
Jin, Y., Andersson, H., Zhang, S., 2016. Air pollution control policies in China: a retrospective and prospects. Int. J. Environ. Res. Publ. Health 13 (12), 1219.
Li, B., Zhang, J., Zhao, Y., Yuan, S.Y., Zhao, Q.Y., Shen, G.F., Wu, H.S., 2015. Seasonal variation of urban carbonaceous aerosols in a typical city Nanjing in Yangtze River Delta, China. Atmos. Environ. 106, 223–231.
Li, M., Zhang, Q., Zheng, B., Tong, D., Lei, Y., Liu, F., Hong, C.P., Kang, S.C., Yan, L., Zhang, Y.X., Bo, Y., Su, H., Cheng, Y.F., He, K.B., 2019. Persistent growth of anthropogenic non-methane volatile organic compound (NMVOC) emissions in China during 1990-2017: drivers, speciation and ozone formation potential. Atmos. Chem. Phys. 19, 8897–8913.
Lin, P., Hu, M., Deng, Z., Slanina, J., Han, S., Kondo, Y., Takegawa, N., Miyazaki, Y., Zhao, Y., Sugimoto, N., 2009. Seasonal and diurnal variations of organic carbon in $PM_{2.5}$ in Beijing and the estimation of secondary organic carbon. J. Geophys. Res. 114, D00G11.
Liu, X.Y., Nie, D.Y., Zhang, K., Wang, Z.Y., Li, X.Q., Shi, Z.H., Wang, Y.Y., Huang, L., Chen, M.D., Ge, X.L., Ying, Q., Yu, X.N., Liu, X.G., Hu, J.L., 2019. Evaluation of particulate matter deposition in the human respiratory tract during winter in Nanjing using size and chemically resolved ambient measurements. Air. Qual. Atmos. Health. 12, 529–538.
Lu, M.H., Zheng, J.Y., Huang, Z.J., Wu, C., Zheng, C.Z., Jia, G.L., Zhang, L.H., Jiang, F., Li, Z., Liu, J.W., Chen, D.H., 2021. Insight into the characteristics of carbonaceous aerosols at urban and regional sites in the downwind area of Pearl River Delta region, China. Sci. Total Environ. 778, 146251.
Millet, D.B., Donahue, N.M., Pandis, S.N., Polidori, A., Stanier, C.O., Turpin, B.J., Goldstein, A.H., 2005. Atmospheric volatile organic compound measurements during the Pittsburgh air quality study: results, interpretation, and quantification of primary and secondary contributions. J. Geophys. Res. Atmos. 110, D07S07.
Mousavi, A., Sowlat, M.H., Lovett, C., Rauber, M., Szidat, S., Boffi, R., Borgini, A., De Marco, C., Ruprecht, A.A., Sioutas, C., 2019. Source apportionment of black carbon (BC) from fossil fuel and biomass burning in metropolitan Milan, Italy. Atmos. Environ. Times 203, 252–261.
NJNBS, 2018. Statistical Yearbook of Nanjing. China Statistics Press in Chinese.
Petit, J.E., Favez, O., Albinet, A., Canonaco, F., 2017. A user-friendly tool for comprehensive evaluation of the geographical origins of atmospheric pollution: wind and trajectory analyses. Environ. Model. Software 88, 183–187.
Qi, X.M., Ding, A.J., Nie, W., Petaja, T., Kerminen, V.M., Herrmann, E., Xie, Y.N., Zheng, L.F., Manninen, H., Aalto, P., Sun, J.N., Xu, Z.N., Chi, X.G., Huang, X., Boy, M., Virkkula, A., Yang, X.Q., Fu, C.B., Kulmala, M., 2015. Aerosol size distribution and new particle formation in the western Yangtze River Delta of China: 2 years of measurements at the SORPES station. Atmos. Chem. Phys. 15, 12445–12464.
Sandrini, S., Fuzzi, S., Piazzalunga, A., Prati, P., Bonasoni, P., Cavalli, F., Bove, M.C., Calvello, M., Cappelletti, D., Colombi, C., Contini, D., de Gennaro, G., Di Gilio, A., Fermo, P., Ferrero, L., Gianelle, V., Giugliano, M., Ielpo, P., Lonati, G., Marinoni, A., Massabò, D., Molteni, U., Moroni, B., Pavese, G., Perrino, C., Perrone, M.G., Perrone, M.R., Putaud, J.-P., Sargolini, T., Vecchi, R., Gilardoni, S., 2014. Spatial and seasonal variability of carbonaceous aerosol across Italy. Atmos. Environ. 99, 587–598.
Schmale, J., Henning, S., Henzing, B., Keskinen, H., Sellegri, K., Ovadnevaite, J., Bougiatioti, A., Kalivitis, N., Stavroulas, I., Jefferson, A., Park, M., Schlag, P., Kristensson, A., Iwamoto, Y., Pringle, K., Reddington, C., Aalto, P., Aijala, M., Baltensperger, U., Bialek, J., Birmili, W., Bukowiecki, N., Ehn, M., Fjaeraa, A.M., Fiebig, M., Frank, G., Frohlich, R., Frumau, A., Furuya, M., Hammer, E., Heikkinen, L., Herrmann, E., Holzinger, R., Hyono, H., Kanakidou, M., Kiendler-Scharr, A., Kinouchi, K., Kos, G., Kulmala, M., Mihalopoulos, N., Motos, G., Nenes, A., O'Dowd, C., Paramonov, M., Petaja, T., Picard, D., Poulain, L., Prevot, A. S., Slowik, J., Sonntag, A., Swietlicki, E., Svenningsson, B., Tsurumaru, H., Wiedensohler, A., Wittbom, C., Ogren, J.A., Matsuki, A., Yum, S.S., Myhre, C.L., Carslaw, K., Stratmann, F., Gysel, M., 2017. Collocated observations of cloud condensation nuclei, particle size distributions, and chemical composition. Sci. Data 4, 170003.
Tang, Y.X., Han, S.Q., Cai, Z.Y., Yang, X., Feng, J., 2019. Feature analysis of atmospheric self-purification capability and atmospheric particulate concentration in Tianjin during 2013-2017. J. Meteorol. Environ. 35, 12.
Tong, D., Cheng, J., Liu, Y., Yu, S., Yan, L., Hong, C.P., Qin, Y., Zhao, H.Y., Zheng, Y.X., Geng, G.N., Li, M., Liu, F., Zhang, Y.X., Zheng, B., Clarke, L., Zhang, Q., 2020. Dynamic projection of anthropogenic emissions in China: methodology and 2015-2050 emission pathways under a range of socio-economic, climate policy, and pollution control scenarios. Atmos. Chem. Phys. 20, 5729–5757.
Turpin, B.J., Huntzicker, J.J., 1995. Identification of secondary organic aerosol episodes and quantitation of primary and secondary organic aerosol concentrations during Scaqs. Atmos. Environ. 29, 3527–3544.
Vedantham, R., Norris, G., Brown, S.G., Roberts, P., 2012. Combining continuous near-road monitoring and inverse modeling to isolate the effect of highway expansion on a school in Las Vegas. Atmos. Pollut. Res. 3, 105–111.

Vodicka, P., Schwarz, J., Cusack, M., Zdimal, V., 2015. Detailed comparison of OC/EC aerosol at an urban and a rural Czech background site during summer and winter. Sci. Total Environ. 518–519, 424–433.

Wang, H., Yan, R., Xu, T., Wang, Y., Wang, Q., Zhang, T., An, J., Huang, C., Gao, Y., Gao, Y., Li, X., Yu, C., Jing, S., Qiao, L., Lou, S., Tao, S., Li, Y., 2020a. Observation constrained aromatic emissions in Shanghai, China. J. Geophys. Res. Atmos. 125, e2019JD031815.

Wang, H.L., An, J.L., Zhu, B., Shen, L.J., Duan, Q., Shi, Y.Z., 2017. Characteristics of carbonaceous aerosol in a typical industrial City-Nanjing in Yangtze River Delta, China: size distributions, seasonal variations, and sources. Atmosphere 8 (4), 73.

Wang, M., Qin, W., Chen, W., Zhang, L., Zhang, Y., Zhang, X., Xie, X., 2020b. Seasonal variability of VOCs in Nanjing, Yangtze River delta: implications for emission sources and photochemistry. Atmos. Environ. 223, 117254.

Wang, P., Cao, J.J., Shen, Z.X., Han, Y.M., Lee, S.C., Huang, Y., Zhu, C.S., Wang, Q.Y., Xu, H.M., Huang, R.J., 2015. Spatial and seasonal variations of $PM_{2.5}$ mass and species during 2010 in Xi'an, China. Sci. Total Environ. 508, 477–487.

Wang, Z., Wang, T., Guo, J., Gao, R., Xue, L.K., Zhang, J.M., Zhou, Y., Zhou, X.H., Zhang, Q.Z., Wang, W.X., 2012. Formation of secondary organic carbon and cloud impact on carbonaceous aerosols at Mount Tai, North China. Atmos. Environ. 46, 516–527.

Wu, C., Wu, D., Yu, J.Z., 2018. Quantifying black carbon light absorption enhancement with a novel statistical approach. Atmos. Chem. Phys. 18, 289–309.

Wu, C., Wu, D., Yu, J.Z., 2019. Estimation and uncertainty analysis of secondary organic carbon using 1 year of hourly organic and elemental carbon data. J. Geophys. Res. Atmos. 124, 2774–2795.

Yang, H., Yu, J.Z., Ho, S.S.H., Xu, J.H., Wu, W.S., Wan, C.H., Wang, X.D., Wang, X.R., Wang, L.S., 2005. The chemical composition of inorganic and carbonaceous materials in $PM_{2.5}$ in Nanjing, China. Atmos. Environ. Times 39, 3735–3749.

Yu, F., 2011. A secondary organic aerosol formation model considering successive oxidation aging and kinetic condensation of organic compounds: global scale implications. Atmos. Chem. Phys. 11, 1083–1099.

Yu, H., Wu, C., Wu, D., Yu, J.Z., 2010. Size distributions of elemental carbon and its contribution to light extinction in urban and rural locations in the pearl river delta region, China. Atmos. Chem. Phys. 10, 5107–5119.

Zhang, P., Ma, P.K., Zhang, H.X., Shu, J.N., Yang, B., Li, Z., 2017. Application of VUV-PIMS coupled with GC-MS in chemical characterization, identification and comparative analysis of organic components in both vehicular-derived SOA and haze particles. Atmos. Environ. 164, 250–258.

Zhang, Q., Zheng, Y., Tong, D., Shao, M., Wang, S., Zhang, Y., Xu, X., Wang, J., He, H., Liu, W., Ding, Y., Lei, Y., Li, J., Wang, Z., Zhang, X., Wang, Y., Cheng, J., Liu, Y., Shi, Q., Yan, L., Geng, G., Hong, C., Li, M., Liu, F., Zheng, B., Cao, J., Ding, A., Gao, J., Fu, Q., Huo, J., Liu, B., Liu, Z., Yang, F., He, K., Hao, J., 2019. Drivers of improved $PM_{2.5}$ air quality in China from 2013 to 2017. Proc. Natl. Acad. Sci. U. S. A 116, 24463–24469.

Zhao, M.F., Huang, Z.S., Qiao, T., Zhang, Y.K., Xiu, G.L., Yu, J.Z., 2015. Chemical characterization, the transport pathways and potential sources of $PM_{2.5}$ in Shanghai: seasonal variations. Atmos. Res. 158, 66–78.

Zheng, B., Tong, D., Li, M., Liu, F., Hong, C.P., Geng, G.N., Li, H.Y., Li, X., Peng, L.Q., Qi, J., Yan, L., Zhang, Y.X., Zhao, H.Y., Zheng, Y.X., He, K.B., Zhang, Q., 2018. Trends in China's anthropogenic emissions since 2010 as the consequence of clean air actions. Atmos. Chem. Phys. 18, 14095–14111.